Regular Article

Synthesis and Aldose Reductase Inhibitory Activity of Botryllazine A Derivatives

Ryota Saito,*[a,b] Kana Ishibashi,[a] Maiko Noumi,[a] Sota Uno,[a] Shoko Higashi,[a] Masaru Goto,[c] Shunsuke Kuwahara,[a,b] and Toshiya Komatsu[d]

[a] *Department of Chemistry, Toho University; 2–2–1 Miyama, Funabashi, Chiba 274–8510, Japan:* [b] *Research Center for Materials with Integrated Properties, Toho University; 2–2–1 Miyama, Funabashi, Chiba 274–8510, Japan:* [c] *Department of Biomolecular Science, Toho University; 2–2–1 Miyama, Funabashi, Chiba 274–8510, Japan: and* [d] *Faculty of Pharmaceutical Sciences, Teikyo Heisei University; 4–21–2 Nakano, Nakano-ku, Tokyo 164–8530, Japan.*
Received January 4, 2019; accepted March 26, 2019

Aldose reductase (AR) is associated with the onset of diabetic complications. Botryllazine A and its analogues were synthesized and evaluated for human AR inhibitory activity. Analogues possessing aromatic bicyclic systems at the C5 position of the central pyrazine ring exhibited superior AR inhibiting activity relative to the parent botryllazine A. In addition, the benzoyl groups at positions C2 and C3 of the pyrazine ring were dispensable for this improved inhibitory activity. Conversely, a benzoyl group—containing phenolic hydroxyl groups—at either position C2 or C3 of the pyrazine ring was essential for attainment of high inhibitory activity approaching that of sorbinil (a highly effective AR inhibitor).

Key words aldose reductase (AR); aldose reductase inhibitor (ARI); diabetic complication; botryllazine A; pyrazine; docking study

Introduction

Diabetes mellitus (DM) is a metabolic abnormality characterized by a steady hyperglycemic state, which can cause severe complications including neuropathy, nephropathy, and retinopathy.[1] Under normoglycemic conditions, most circulating glucose molecules are metabolized *via* glycolysis to produce ATP, while only approximately 5% are metabolized *via* the polyol pathway (in which glucose is reduced to sorbitol by reduced nicotinamide adenine dinucleotide phosphate (NADPH)-requiring aldose reductase (AR), followed by conversion of sorbitol to fructose by NAD^+-requiring sorbitol dehydrogenase (SDH))[2,3] (Fig. 1). Hyperglycemic conditions, however, overwhelm the glycolytic system and activate AR to convert excess glucose into sorbitol, elevating flux through this alternate pathway (under hyperglycemic conditions, 11% of glucose is metabolized *via* the polyol pathway in human erythrocytes).[3] Because the sorbitol to fructose conversion rate remains unchanged (*i.e.*, lags behind sorbitol formation), and highly hydrophilic sorbitol cannot easily diffuse across cell membranes, an abnormal accumulation of intracellular sorbitol leads to osmotic stress. In addition, chronic acceleration of the polyol pathway results in an increased level of advanced glycation end products (AGEs), formed by reaction of proteins with accumulating fructose, thereby favoring eventual development of diabetic complications.[2,3]

Inhibition of AR has thus been considered a useful strategy for attenuating development of diabetic complications. Various AR inhibitors (ARIs) have been developed, and most highly potent ARIs contain either a glycine unit ($-NHCH_2COOH$) or a spirohydantoin skeleton as key structures.[4] Under conditions of physiological pH, protons dissociate from such functional groups, and resulting corresponding conjugate bases tightly bind the AR active site *via* hydrogen-bonding interactions.[4] However, unfavorable adverse effect profiles, low efficacy, and toxicity have resulted in most compounds exhibiting such architecture being inappropriate for clinical use.[5–9] Thus, development of alternate high-potency ARIs is desirable. In the present study, we focused on the phenolic hydroxyl groups of botryllazines A and B derived from *Botryllus leachi*.[10] These compounds possess electron-withdrawing pyrazine or carbonyl groups at the *p*-position of the phenolic hydroxyl groups, favoring proton dissociation and formation of phenolate anions capable of interacting with the AR active site at physiological pH. Based on this idea, we have previously synthesized and evaluated the AR inhibitory activity of botryllazine B and its derivatives.[11] However, no ARI structure–activity relationship (SAR) study of botryllazine A has been conducted. In the present study, we have thus synthesized several botryllazine

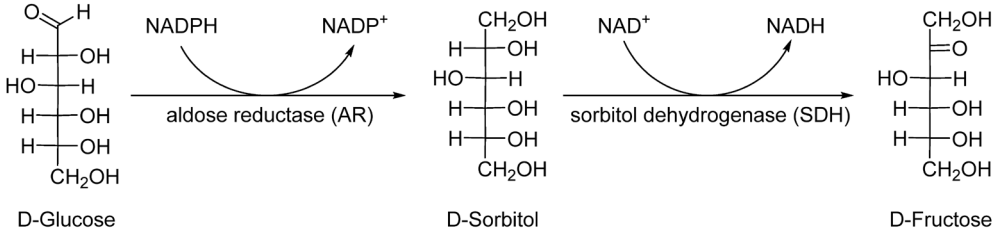

Fig. 1. Polyol Pathway of Glucose Metabolism

* To whom correspondence should be addressed. e-mail: saito@chem.sci.toho-u.ac.jp

A derivatives (Fig. 2) and evaluated their inhibitory activities against recombinant human AR, thereby providing the first SAR data for this family of compounds.

Results and Discussion

The synthesis of botryllazine A and its derivatives (Fig. 2: **1a**–**c**) were started from 2,3-dichoropyrazine, which was lithiated using lithium tetramethylpiperidide (LiTMP), followed by reaction with anisaldehyde to produce the corresponding alcohol **3**, as shown in Chart 1.[12] These steps were repeated to produce a diol **4**,[12] which was oxidized using 2-iodoxybenzoic acid (IBX) to produce an unpurified intermediate **5**. A Suzuki–Miyaura coupling reaction using appropriate boronic acids produced further intermediates **6a**–**c**.

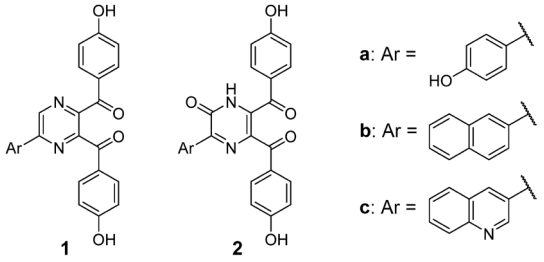

Fig. 2. Structures of Botryllazine A (**1a**) and Derivatives (**1b**, **1c**, and **2a**–**c**) Examined during the Present Study

Initially, reductive dechlorination of **6a** was attempted using the method reported by Buron *et al.*[12] However, this approach produced a low yield (4.3%) of desired product **7a**, while undesired pyrazinone derivative **8a** was the major product (Table 1, entry 1). The formation of **8a** was apparently due to participation of a small volume of water—added to the catalyst Pd/C to avoid spontaneous combustion—in the reaction. It thus appears that the quality or condition of the catalyst significantly influences the reaction. In order to minimize participation of water in the reaction, a dried matrix-embedded Pd/C catalyst

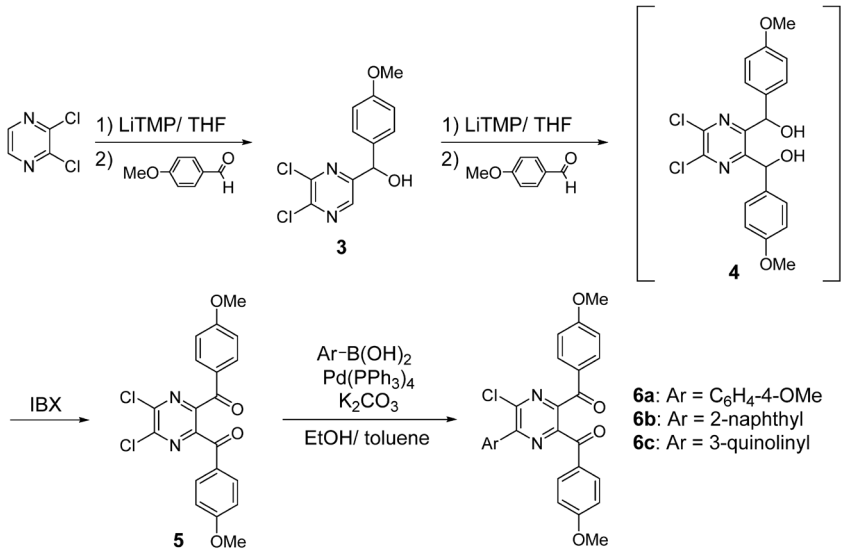

Chart 1. Synthesis of Key Intermediates **6a**–**c** *en Route* to Production of Botryllazine A and Its Derivatives

Table 1. Optimizing Reductive Dechlorination of **6a**–**c**

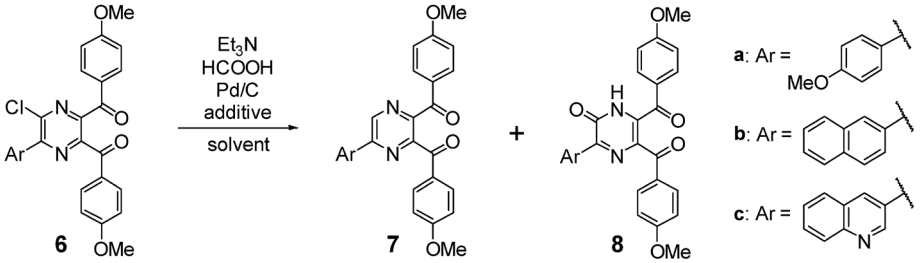

Entry	Chloride	Equivalent of Pd/C	Solvent[a]	Hydrogen source	Additive	Yield	
1	**6a**	0.1	Acetone	HCOOH	—	**7a** (4.3%)	**8a** (61%)
2	**6a**	0.1[b]	Acetone	HCOOH	—	**7a** (42%)	**8a** (37%)
3	**6a**	0.1[b]	Acetone	HCOOH	—	—	—
4	**6a**	0.1[b]	THF	HCOOH	—	—	—
5	**6a**	0.1[b]	Acetone	HCOOH	MS3A	**7a** (29%)	—
6	**6a**	0.05	Acetone	HCOOH	—	**7a** (20%)	**8a** (19%)
7	**6b**	0.05	Acetone	HCOOH	—	**7b** (—)	**8b** (54%)
8	**6c**	0.05	Acetone	HCOOH	—	**7c** (54%)	**8c** (37%)

a) All solvents were dehydrated. *b*) Matrix carbon, dry-support (purchased from Sigma-Aldrich).

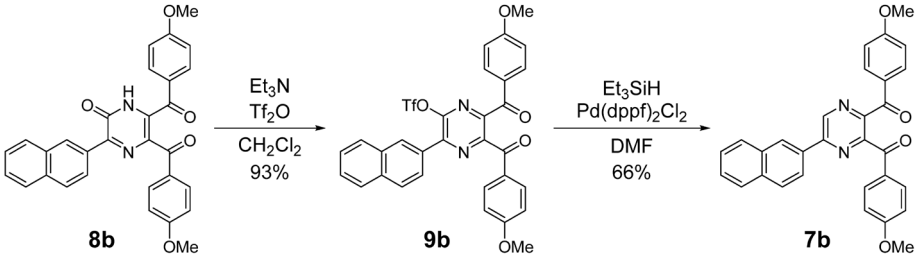

Chart 2. Dehydroxylation Reactions of **8b**

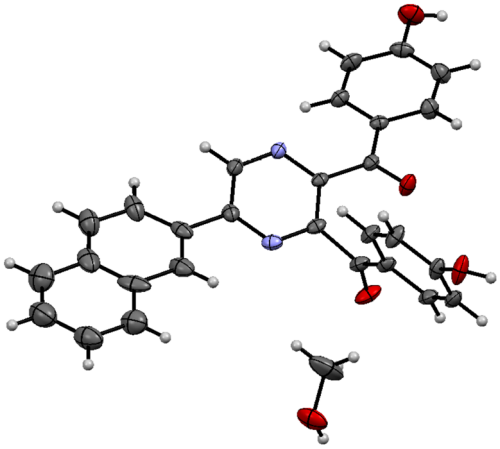

Fig. 3. An ORTEP Diagram of **1b**

(Color figure can be accessed in the online version.)

was employed (Table 1, entry 2). While this improved the yield (42%) of **7a**, a significant quantity of the hydroxylated product **8a** was still formed. When examining the effects of solvent-mediated drying (Table 1, entries 3 and 4) the reaction failed to proceed altogether. Instead, addition of a 3 Å molecular sieve to the reaction mixture successfully enhanced anhydrous conditions and suppressed formation of pyrazinone **8a**, but also depressed the yield (29%) of **7a** (Table 1, entry 5). Another dechlorination condition—using triethylsilane as the hydrogen source, in combination with palladium acetate[13]—yielded no improvement (data not shown). Using the original condition in conjunction with a lower Pd/C concentration (0.05 eq instead of 0.1 eq) (Table 1, entry 6), **6c** conversion still resulted in the hydroxylated product, but the yield of **7c** improved (54%) (Table 1, entry 8). We thus concluded that, during palladium-catalyzed dechlorination of structure **6**-type chloropyrazines, formation of the hydroxylation product could be only partially attenuated, and only an unsatisfactory improvement in yield of the desired reaction products was achievable.

We therefore adopted a new synthetic strategy (conversion of the hydroxylated products) to obtain **7b** (Chart 2). This approach first converted the pyrazinone **8b** into the corresponding triflate **9b**, which were then successfully reduced *via* the triethylsilane-Pd(dppf)$_2$Cl$_2$ system,[14–17] providing a satisfactory yield of **7b** (Chart 2). Fortunately, 2-naphthyl derivative **1b** provided single crystals suitable for X-ray crystallographic analysis. The structure was successfully solved (Fig. 3), unambiguously confirming successful dehydroxylation of the C6-hydroxylated byproducts.

Obtained products **7a**–**c** were then subjected to pyridinium chloride-mediated deprotection to produce botryllazine A and its analogues **1a**–**c** (Table 2). Pyrazinones **8a**–**c** were also subjected to the same deprotection reactios to produce **2a**–**c**, the corresponding C6-hydroxylated derivatives of **1a**–**c** (Table 2).

Table 2. Demethylation Reactions of **7a**–**c** and **8a**–**c**

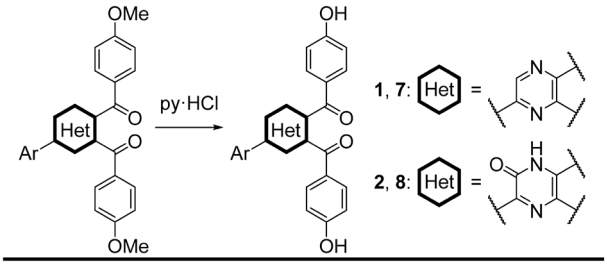

entry	substrate	Ar	product (yield)
1	**7a**	MeO	**1a** (30%)
2	**7b**		**1b** (66%)
3	**7c**	N	**1c** (16%)
4	**8a**	MeO	**2a** (20%)
5	**8b**		**2b** (34%)
6	**8c**	N	**2c** (13%)

We also synthesized compound **10**, which is a position isomer of botryllazine B, to investigate the effect of the C3 substituent in botryllazine A (**1a**). The synthetic route is shown in Chart 3. 5-(4-Methoxyphenyl)pyrazine-2-carboxylic acid (**11**)[18] was first converted into amide **12**, which was reacted with 4-methoxyphenylmagnisiumbromide to give **13**. Then, methyl protecting groups in **13** were deprotected with pyridinium chloride to afford **10**.

The AR inhibitory activities of **1a**–**c**, **2a**–**c**, and **10** were evaluated *in vitro*, by measuring inhibition of human AR-mediated D,L-glyceraldehyde reduction in the presence of cofactor NADPH.[19] Consumption of NADPH—a validated and reliable proxy for progress of this reaction—was spectrophotometrically monitored.[11] Inhibitory activities were quantitatively expressed as IC$_{50}$ values. Results are shown in Table 3, accompanied by reference IC$_{50}$ values of botryllazine B and epalrestat.

The IC$_{50}$ value of botryllazine A (**1a**) was estimated at

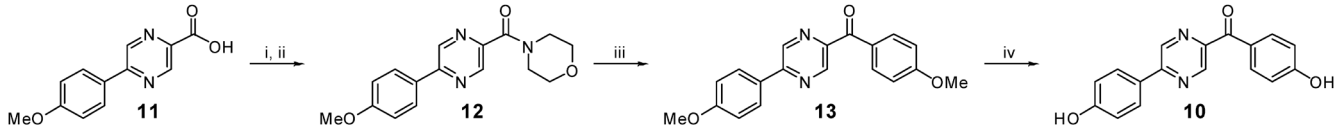

Reagents and conditions: (i) thionyl chloride, reflux; (ii) morpholine, CH_2Cl_2, 0°C to r.t.; (iii) 4-(OMe)C_6H_4MgBr, THF, −100°C to r.t., then H_3O^+; (iv) pyridinium chloride, 210°C.

Chart 3. Synthesis of Compound **10**

Table 3. *In Vitro* AR Inhibitory Activities of Botryllazine A Derivatives (**1a**–**c** and **2a**–**c**), Botryllazine B, **10**, and Epalrestat

Inhibitor	IC_{50} (μM)
1a	6.47±2.42
1b	4.60±1.22
1c	4.03±0.08
2a	9.64±2.07
2b	5.85±0.94
2c	1.34±0.24
10	1.66±0.66
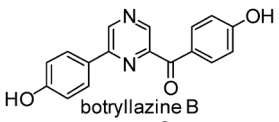 botryllazine B	1.55[a]
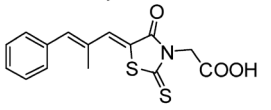 epalrestat	0.092±0.028

[a] Datum was taken from Ref 11.

6.47 μM, an approximately 3-fold higher level of inhibitory activity than previously-reported (19.4 μM).[20] Such disagreement likely results from differences in experimental conditions. In the present study, the bioassay was carried out in a 1 cm quartz cell (total volume 1.0 mL) at 25°C, while previous studies employed 96-well microtiter plates (total volume 0.2 mL) at 37°C.[20] Furthermore, enzyme concentration in the present study (1.0–1.2 U/mL) differed from that in the previous study (0.5 mU/mL). However, since the IC_{50} value of positive control epalrestat estimated by the present study agrees with previously-reported values, this verifies that current study experimental data represent absolute values.

All examined compounds exhibited high inhibitory activity, with IC_{50} values in the range of 1.34–9.64 μM (*i.e.*, comparable to that of sorbinil, a highly-effective AR inhibitor).[9,21] Introducing a bicyclic heterocycle substituent at the C5 position marginally enhanced inhibitory activity (**1b**, **1c**, **2b**, and **2c**), but the presence of a hydroxy group at the C6 position did not markedly alter inhibitory activity (activity comparison of **2a**–**c**—which possess a C6 hydroxy group—with corresponding C6-unhydroxylated **1a**–**c**). Furthermore, removal of the hydroxybenzoyl group at the C2 position resulted in an increment in inhibitory activity (botryllazine B[11] *versus* **1a**), suggesting that a second benzoyl group (in addition to the one present at the C3 position) is dispensable for enhanced AR inhibitory activity. Moreover, removal of the hydroxybenzoyl group from the C3 position of **1a** also resulted in an increment of the inhibitory activity (**10** *vs.* **1a**), and the IC_{50} value was almost the same as that of botryllazine B,[11] suggesting that two benzoyl groups on C2 and C3 are unnecessary and only one benzoyl group on either C2 or C3 is effective for gaining high AR inhibitory activity.

To develop an understanding of the relationship between botryllazine A analogue structure and AR inhibitory activity, docking studies were carried out using known human AR X-ray crystal structures. Reported AR crystal structures demonstrate that the active site can be divided into three subregions: catalytic, hydrophobic, and specificity pockets. The catalytic pocket, also referred to as an anion-binding pocket, is composed of Tyr48, His110, Trp20, and Trp111 side chains, and is positioned in proximity to cofactor NADPH. Key structures (glycine units and spirohydantoins) of the highly potent ARIs bind this pocket in their conjugate base forms at physiological pH. The adjacent hydrophobic pocket is composed of Trp20, Phe122, and Trp219 residues; therefore, a requirement of highly potent ARIs is the presence of a hydrophobic moiety in addition to their acidic groups.[4,9,22–24] The specificity pocket is adjacent to the other two pockets,[4] and has a flexible structure to accommodate various ligands with diverse structures, whereas architecture of the catalytic pocket is near-identical in most reported crystal structures. This ligand-induced-fit function is achieved by movement of the Cys298–Cys303 loop region, such that AR is able to assume two distinct specificity pocket states (based on the position of these residues): "open" and "closed."[24] While hundreds of crystal structures of human AR containing various kinds of inhibitors have been registered with the Protein Data Bank (PDB), AR ligand-binding modes can be classified into five types (PDB structures 1PWM, 1Z3N, 2FZD, 2NVC, and 2NVD) based on specificity pocket state (open or closed) and ligand orientation in the active site.[25,26] These PDB structures are frequently used in AR docking studies,[24,27,28] and were thus employed by the present study as well. The present study employed one additional crystal structure recently reported by Klebe and colleagues (PDB ID: 4IGS),[29] given that the binding moiety of the ligand in this structure is a phenolic hydroxy group (considered a key structure by the present study).

Prior to carrying out docking simulations, ligand optimized structures and atom charges were calculated using the PM7 method.[30–32] All docking experiments were performed using GOLD Suite software.[33,34] The ChemPLP scoring function[35] was used to predict docking poses for each of the six specificity pocket states, and these were then rescored using the Astex

Table 4. Astex Statistical Potential (ASP) Fitness Scores for Docking of **1a–c**, **2a–c**, and Botryllazine B with Six Different Protein Data Bank (PDB) Protein Structures, Including Their Correlation (r^2) with Empirical pIC_{50} Values

Compound	Protein structure (state of the specificity pocket)					
	1PWM (closed)	1Z3N (open)	2FZD (open)	2NVC (closed)	2NVD (closed)	4IGS (closed)
1a	115.5816	100.8451	110.3716	107.1515	91.8687	105.4701
1b	117.2774	115.0713	104.9774	109.2310	99.4169	107.2104
1c	121.7395	109.9514	107.417	111.3878	96.1964	109.1394
2a	115.1591	109.3466	109.7031	110.6786	93.6458	104.3201
2b	121.0703	115.0403	107.5076	110.1408	98.1937	108.4239
2c	125.6161	117.0648	107.4877	112.6584	100.4004	113.1883
Botryllazine B	108.2904	97.7533	105.9444	100.7796	105.9115	94.6767
r	0.761	0.306	0.169	0.373	0.510	0.910

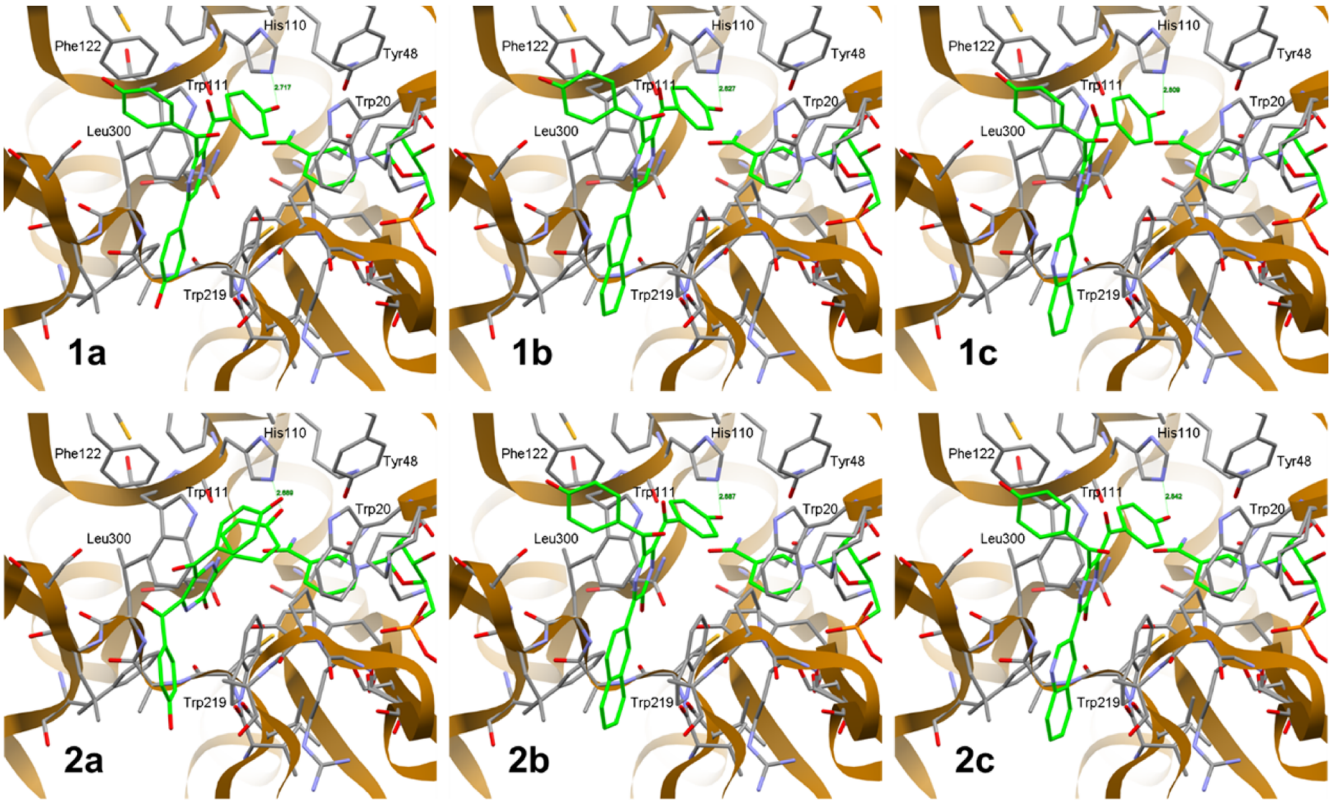

Fig. 4. Predicted Binding Modes for **1a–c** and **2a–c** Docked into 4IGS
(Color figure can be accessed in the online version.)

Statistical Potential (ASP)[36] scoring function, validated for protein-ligand specific hydrogen bond scoring.[37] The combination of these scores was used to determine the optimal pose of each ligand (*i.e.*, for which both scoring functions yielded positive, high scores) (Table 4).

Botryllazine B, which exhibited high AR inhibitory activity, yielded lower docking scores than the other ligands. This is attributed to the smaller molecular size of botryllazine B (producing fewer points of interaction with the AR active site) relative to the botryllazine A derivatives (**1a–c** and **2a–c**), making direct comparison of their docking scores meaningless. However, comparison of botryllazine A derivatives' docking scores is of utility, given their strong structural resemblances. Closer examination of **1a–c** and **2a–c** docking scores demonstrated that almost all compounds exhibited optimal fit with the 1PWM AR structure. However, correlation between docking scores and experimental pIC_{50} values was poor ($r = 0.761$), whereas a strong correlation was observed for the 4IGS AR structure ($r = 0.910$). A possible criticism is that the GOLD analysis should consider "flexible" dockings using the software's Side Chain Flexibility function, but we previously demonstrated that the better method for predicting an appropriate protein structure that accounts for experimental results is assessment of the docking score-pIC_{50} correlation.[38]

Docking positions for **1a–c** and **2a–c** with 4IGS demonstrated that **2a**, which exhibited the lowest inhibitory activity of the examined botryllazine A derivatives, was predicted to assume a different position relative to the other derivatives (Fig. 4). The hydroxy group of the C5 phenol of **2a** forms a hydrogen bond with His110 of the catalytic pocket, while the other derivatives form hydrogen bonds with His110 *via* the hydroxy group of the C2 benzoyl groups (reinforced by C5

aryl scaffolds adjacent to Trp219 of the hydrophobic pocket). According to our previous pharmacophore modeling analysis of 4IGS, a lipophilic interaction with Trp219 is an important feature conferring additional inhibitory activity.[38] Indeed, the quinolin-3-yl residue of compound **1c**, the most potent among **1a–c**, forms a π–π interaction with the indole ring of Trp219. The naphthalen-2-yl group of **1b** also occurs in proximity to Trp219, and the same trend is observed for **2b** and **2c**. Based on these results, we conclude that an aromatic face-to-face interaction between the C5 aromatic ring of a botryllazine A derivative and the hydrophobic pocket Trp219 residue—as well as hydrogen bonding between one hydroxybenzoyl group and the catalytic pocket His110—enhances AR inhibitory activity of botryllazine A-based compounds.

Conclusion

In the present study, botryllazine A derivatives were synthesized and evaluated for AR inhibitory activity. The previously-reported botryllazine A preparation method proved irreproducible, and thus an alternative synthetic route involving dehydroxylation was established. Botryllazine A was originally reported to exhibit higher AR inhibitory activity than botryllazine B.[20] In disagreement with this, the present study demonstrated that botryllazine A derivatives are less potent than corresponding botryllazine B derivatives, but they do exhibit inhibitory activities comparable to that of the highly-effective AR inhibitor sorbinil. Furthermore, introducing a quinoline ring at the C5 position enhances AR inhibitory activity. As indicated by the higher IC_{50} values obtained for botryllazine B than botryllazine A derivatives, having two *para*-hydroxybenzoyl groups (*i.e.*, at *both* the C2 and C3 positions of the central pyrazine ring) is dispensable for high AR inhibitory activity. The docking study suggests that the botryllazine A derivative series molecules enter the AR active site when the specificity pocket is in its closed state. Furthermore, it appears that under such circumstances a π–π interaction—between inhibitor bicyclic systems at the C5 position and the hydrophobic pocket Trp219 residue—plays an important role in conferring enhanced AR inhibitory activity. These results provide important insights which will contribute towards the design of novel botryllazine-based AR inhibitors.

Experimental

General NMR spectra were recorded on a JNM-ECP400 spectrometer (JEOL Ltd., Japan). Chemical shifts (δ) are reported in ppm using tetramethylsilane or an undeuterated solvent as internal standards in the deuterated solvent used. Coupling constants (J) are given in Hz. Chemical shift multiplicities are reported as s = singlet, d = doublet, t = triplet, m = multiplet. FAB mass spectra were taken on a JMS-600-H mass spectrometer (JEOL Ltd., Japan). Xenon was used as a bombardment gas, and all analyses were carried out in positive mode with the ionization energy and the accelerating voltage set at 70 eV and 3 kV, respectively. A mixture of dithiothreitol (DTT) and α-thioglycerol (TG) (1 : 1) was used as a liquid matrix. High-resolution electrospray ionization (HR-ESI)-MS were measured on a JEOL Model JMS-T100CS mass spectrometer. All conventional chemicals used in the present study are commercially available and were used as received. Column chromatography was carried out on silica gel (particle size; 46–50 μm; Fuji Silysia Chemical Ltd.).

Synthesis of 2,3-Dichloro-5,6-bis(1-oxo-4-methoxyphenylmethyl)pyrazine (5) A solution of *n*-BuLi in hexane (2.6 M, 18.0 mL, 46.8 mmol) was added to stirred anhydrous tetrahydrofuran (THF) (30 mL) at −40°C under an atmosphere of Ar. Then, 2,2,6,6-tetramethylpiperidine (8.2 mL, 48.2 mmol) was added to the solution. The mixture was warmed to 0°C. After 30-min stirring at this temperature, the mixture was cooled to −80°C and a solution of **3** (2.69 g, 9.43 mmol) in THF (5.0 mL) was added. After 30 min at −80°C, *p*-anisaldehyde (1.3 mL, 10.7 mmol) dissolved in THF (0.5 mL) was added and the stirring was continued for 4h at −80°C. The crude product was treated with a solution of saturated sodium hydrogenosulfite (20 mL). The mixture was filtrated and the residue was washed with dichloromethane (DCM). After separating the organic and aqueous phases, the aqueous layer was extracted with DCM (3 × 20 mL). The combined organic extracts were then dried over sodium sulfate and evaporated. To the crude product in MeCN (45.0 mL) was added IBX (6.60 g, 23.6 mmol) at room temperature. After 17 h, the reaction mixture was filtered through a pad of celite using DCM as the eluent, and concentrated. The crude product was purified by column chromatography on silica gel (eluent, $CHCl_3$) to afford **5** as yellow solid (1.90 g, 48%). ^{1}H-NMR ($CDCl_3$, 400 MHz) δ: 7.94 (4H, d, J = 8.7 Hz), 6.95 (4H, d, J = 8.7 Hz), 3.85 (6H, s). ^{13}C-NMR ($CDCl_3$, 100 MHz) δ: 188.3, 164.7, 150.5, 146.4, 133.2, 127.6, 114.1, 55.7. FAB-MS (matrix: DTT/TG = 1/2) m/z: 417 ($[M+H]^+$). These spectral data were in good accordance with those reported previously.[12]

Synthesis of 2-Chloro-3-(naphthalen-2-yl)-5,6-bis(1-oxo-4-methoxyphenylmethyl)pyrazine (6b) A mixture of **5b** (1.50 g, 3.60 mmol), 2-naphtaleneboronic acid (620 mg, 361 mmol), $Pd(PPh_3)_4$ (282 mg, 180 μmol), aqueous 2 M potassium carbonate (3.4 mL, 6.80 mmol) and ethanol (1.1 mL) in toluene (17 mL) was heated to reflux under Ar for 17 h. After cooling to room temperature, the reaction mixture was diluted with 3 mL of a mixture of water and $CHCl_3$ (1 : 1) and the organic layer was separated. The aqueous layer was extracted with $CHCl_3$ (3 × 20 mL). The combined organic extracts were dried over sodium sulfate and evaporated. The crude product was purified by column chromatography on silica gel (eluent; hexane–AcOEt = 7 : 3) to afford **6b** as yellow solid (1.19 g, 65%). ^{1}H-NMR ($CDCl_3$, 400 MHz) δ: 8.48 (1H, s), 8.07 (2H, d, J = 8.8 Hz), 8.03 (2H, d, J = 8.8 Hz), 7.99–7.89 (4H, m), 7.60–7.54 (2H, m), 6.99 (2H, d, J = 8.8 Hz), 6.94 (2H, d, J = 8.8 Hz), 3.89 (3H, s), 3.86 (3H, s). ^{13}C-NMR ($CDCl_3$, 100 MHz) δ: 189.9, 189.2, 164.5, 164.4, 151.6, 149.9, 145.5, 134.0, 133.4, 133.3, 132.8, 132.4, 130.5, 129.0, 128.3, 128.3, 128.1, 127.8, 126.4, 114.1, 114.0, 77.3, 55.7, 55.64. ESI-MS m/z: 531.1073 (Calcd for $C_{30}H_{21}ClN_2NaO_4$ $[M+Na]^+$: 531.1082).

Synthesis of 2-Chloro-3-(quinolin-3-yl)-5,6-bis(1-oxo-4-methoxyphenylmethyl)pyrazine (6c) This material was prepared from **5c** (202.3 mg, 485 μmol) with 3-quinolineboronic acid (74.8 mg, 432 μmol) in a procedure analogous to that for obtaining **6b**. The product was obtained as yellow solid (90.6 mg, 37%). ^{1}H-NMR ($CDCl_3$, 400 MHz) δ: 9.45 (1H, d, J = 2.0 Hz), 8.81 (1H, s), 8.19 (1H, d, J = 8.4 Hz), 8.08–8.02 (4H, m), 7.96 (1H, d, J = 8.0 Hz), 7.85 (1H, t, J = 7.4 Hz), 7.66 (1H, t, J = 7.4 Hz), 7.02–6.95 (4H, m), 3.91 (3H, s), 3.88 (3H, s). ^{13}C-NMR ($CDCl_3$, 100 MHz) δ: 189.6, 188.9, 164.6, 164.5, 151.1, 150.9, 150.3, 148.9, 148.4, 145.7, 137.9, 133.3, 133.2, 131.3, 129.5, 128.8, 128.1, 127.6, 114.1, 114.0, 55.7. ESI-

MS *m/z*: 532.1046 (Calcd for $C_{29}H_{20}ClN_3NaO_4$ $[M+Na]^+$: 532.1040).

A General Procedure for the Reductive Dechlorination Reactions of Chloropyrazines 6 In a flask was placed a solution of **6** (2.19 mmol), triethylamine (20.8 mmol), formic acid (10.6 mmol) and Pd/C (10%) (0.1 or 0.05 eq) in an anhydrous solvent (23 mL) and the mixture was heated at refluxing temperature for 3 h. After cooling to room temperature, the reaction mixture was filtrated by celite, then water (20 mL) and $CHCl_3$ (20 mL) were added to the reaction mixture and separated. The aqueous layer was extracted with $CHCl_3$ (3×20 mL). The combined organic extracts were then dried over sodium sulfate and evaporated. The crude product was purified by column chromatography on silica gel (eluent; $CHCl_3$–AcOEt = 49 : 1) to afford **7** and **8** with yields shown in Table 1.

2,3-Bis(1-oxo-4-methoxyphenylmethyl)-5-(4-methoxyphenyl)pyrazine (7a) was obtained as yellow solid; ^{1}H-NMR ($CDCl_3$, 400 MHz) δ: 9.09 (1H, s), 8.04 (6H, m), 7.00 (6H, m), 3.88 (9H, s). ^{13}C-NMR ($CDCl_3$, 100 MHz) δ: 191.3, 190.8, 164.1, 162.1, 153.2, 150.9, 149.2, 139.0, 133.3, 129.1, 128.6, 127.5, 114.8, 113.9, 113.8, 55.6. FAB-MS (matrix: DTT/TG = 1/1) *m/z*: 455 ($[M+H]^+$). These data were in good accordance with those reported previously.[12]

3-(4-Methoxyphenyl)-5,6-bis(1-oxo-4-methoxyphenylmethyl)pyrazin-2(1*H*)-one (8a) was obtained as yellow solid; ^{1}H-NMR ($CDCl_3$, 400 MHz) δ: 8.49 (2H, d, $J=8.8$ Hz), 8.01 (2H, d, $J=8.8$ Hz), 7.79 (2H, d, $J=8.4$ Hz), 6.97–6.92 (4H, m), 6.85 (2H, d, $J=8.8$ Hz), 3.90 (3H, s), 3.89 (3H, s), 3.83 (3H, s). ^{13}C-NMR ($CDCl_3$, 100 MHz) δ: 188.4, 186.5, 164.6, 163.7, 162.0, 155.0, 150.4, 137.5, 133.2, 132.5, 131.2, 129.2, 128.3, 127.524, 114.326, 113.6, 113.5, 77.4, 77.1, 76.8. ESI-MS *m/z*: 471.1573 (Calcd for $C_{27}H_{23}N_3N_2O_6$ $[M+H]^+$: 471.1556).

3-(Naphthalen-2-yl)-5,6-bis(1-oxo-4-methoxyphenylmethyl)pyrazin-6(1*H*)-one (8b) was obtained as yellow solid; ^{1}H-NMR ($CDCl_3$–methanol-d_4 = 4 : 1, 400 MHz) δ: 9.06 (1H, s), 8.20 (1H, d, $J=8.4$ Hz), 7.99 (6H, d, $J=8.8$ Hz), 7.80 (1H, d, $J=8.8$ Hz), 7.76–7.70 (4H, m), 7.41–7.35 (2H, m), 6.82 (2H, d, $J=8.8$ Hz), 6.79 (2H, d, $J=8.4$ Hz), 3.75 (3H, s), 3.70 (3H, s). ^{13}C-NMR ($CDCl_3$, 100 MHz) δ: 188.7, 187.1, 164.5, 163.6, 155.3, 141.1, 134.2, 133.2, 132.8, 132.2, 131.6, 130.2, 129.3, 128.9, 128.0,127.8, 127.5, 126.2, 125.1, 114.2, 113.4, 77.4, 55.4, 55.3. ESI-MS *m/z*: 513.1432 (Calcd for $C_{30}H_{22}N_2NaO_5$ $[M+Na]^+$: 513.1421).

2,3-Bis(1-oxo-4-methoxyphenylmethyl)-5-(quinolin-3-yl)pyrazine (7c) was obtained as yellow solid; ^{1}H-NMR ($CDCl_3$, 400 MHz) δ: 9.64 (1H, d, $J=1.8$ Hz), 9.33 (1H, s), 8.90 (1H, d, $J=1.8$ Hz), 8.18 (2H, d, $J=8.0$ Hz), 8.07 (2H, d, $J=8.0$ Hz), 8.06 (2H, d, $J=8.0$ Hz), 7.96 (1H, d, $J=8.0$ Hz), 7.82 (1H, t, $J=8.0$ Hz), 7.64 (1H, t, $J=8.0$ Hz), 6.97 (4H, d, $J=8.8$ Hz), 3.89 (6H, s). ^{13}C-NMR ($CDCl_3$, 100 MHz) δ: 190.8, 190.6, 164.3, 153.5, 150.9, 151.2, 148.9, 148.6, 139.9, 135.2, 133.3, 133.2, 131.3, 129.5, 128.9, 128.4, 127.8, 127.7, 127.6, 114,0, 113.9, 55.7. ESI-MS *m/z*: 498.1404 (Calcd for $C_{29}H_{20}N_3NaO_4$ $[M+Na]^+$: 498.1430).

5,6-Bis(1-oxo-4-methoxyphenylmethyl)-3-(quinolon-3-yl)pyrazin-2(1*H*)-one (8c) was obtained as yellow solid; ^{1}H-NMR (DMSO-d_6, 400 MHz) δ: 9.75 (1H, d, $J=2.4$ Hz), 9.62 (1H, d, $J=2.4$ Hz), 8.12 (1H, d, $J=8.0$ Hz), 8.08 (2H, d, $J=8.8$ Hz), 7.97 (1H, d, $J=8.0$ Hz), 7.84 (2H, d, $J=8.8$ Hz), 7.83 (1H, t, $J=8.0$ Hz), 7.61 (1H, t, $J=8.0$ Hz), 6.96 (2H, d, $J=8.8$ Hz), 6.87 (2H, d, $J=8.8$ Hz), 3.89 (3H, s), 3.82 (3H, s). ^{13}C-NMR (DMSO-d_6, 100 MHz) δ: 188.7, 187.4, 164.5, 163.6, 156.4, 150.5, 148.0, 136.7, 133.4, 132.3, 131.9, 131.3, 129.8, 129.4, 128.8, 128.7, 127.8, 127.3, 114.9, 114.8, 114.4, 114.1, 56.3, 56.1. ESI-MS *m/z*: 513.1387 (Calcd for $C_{29}H_{21}N_3NaO_5$ $[M+Na]^+$: 514.1373).

Synthesis of 2,3-Bis(1-oxo-4-methoxyphenylmethyl)-5-(naphthalen-2-yl)-6-trifluoromethanesulfonylpyrazine (9b) Triethylamine (0.13 mL, 933 μmol) and trifluoromethanesulfonic anhydride (0.14 mL, 832 μmol) were added to a DCM solution (3.8 mL) of **8b** (400 mg, 865 μmol) and stirred for 2 h. Then water (15 mL) and $CHCl_3$ (15 mL) were added to the reaction mixture and separated. The aqueous layer was extracted with $CHCl_3$ (3×15 mL). The combined organic extracts were then dried over sodium sulfate and evaporated. The crude product was purified by column chromatography on silica gel (eluent; chloroform) to afford **9b** as yellow solid (502 mg, 93%). ^{1}H-NMR ($CDCl_3$, 400 MHz) δ: 8.61 (1H, s), 8.15–8.11 (3H, m), 8.04–7.96 (4H, m), 7.91 (1H, d, $J=7.6$ Hz), 7.60 (2H, quint, $J=7.6$ Hz), 6.99 (4H, t, $J=8.6$ Hz), 3.90 (3H, s), 3.87 (3H, s). ^{13}C-NMR ($CDCl_3$, 100 MHz) δ: 189.7, 188.1, 164.7, 164.5, 153.6, 147.6, 147.3, 144.6, 134.6, 133.6, 133.2, 133.0, 130.8, 129.3, 129.3, 129.0, 128.4, 128.2, 127.9, 127.6, 127.1, 125.6, 123.24, 120.0, 116.9, 113.7, 55.7. ESI-MS *m/z*: 645.0901 (Calcd for $C_{31}H_{21}F_3N_2NaO_7S$ $[M+Na]^+$: 645.0914).

Synthesis of 2,3-Bis(1-oxo-4-methoxyphenylmethyl)-5-(naphthalen-2-yl)pyrazine (7b) To a mixture of **9b** (400 mg, 643 μmol), $Pd(dppf)_2Cl_2$ (24.1 mg, 32.9 μmol) in 1.5 mL of anhydrous DMF at 60°C was added triethylsilane (0.25 mL, 1.57 mmol). After 6 h, the mixture was successively washed with water (30 mL). The aqueous layer was extracted with $CHCl_3$ (3×30 mL). The combined organic extracts were then dried over sodium sulfate and evaporated. The crude product was purified by column chromatography on silica gel (eluent; $CHCl_3$) to afford **7b** as yellow solid (183 mg, 60%). ^{1}H-NMR ($CDCl_3$, 400 MHz) δ: 9.28 (1H, s), 8.61 (1H, s), 8.20 (1H, d, $J=8.8$ Hz), 8.10–8.06 (4H, m), 7.97–7.94 (2H, m), 7.87 (1H, d, $J=6.8$ Hz), 7.57–7.54 (2H, m), 6.98–6.96 (4H, m), 3.86 (3H, s). ^{13}C-NMR ($CDCl_3$, 100 MHz) δ: 191.2, 190.8, 164.2, 153.3, 151.1, 150.2, 140.0, 134.5, 133.4, 133.2, 132.3, 129.2, 129.1, 128.6, 128.6, 127.9, 127.9, 127.8, 127.0, 124.1, 114.0, 113.9, 77.4, 55.6. ESI-MS *m/z*: 497.1460 (Calcd for $C_{30}H_{22}N_2NaO_4$ $[M+Na]^+$: 497.1472).

Synthesis of Botryllazine A (1a)[12] This material was prepared by the literature method, and all the spectral data were in good accordance with those reported previously.[12] ^{1}H-NMR (methanol-d_4, 400 MHz) δ: 9.21 (1H, s), 8.08 (2H, d, $J=8.4$ Hz), 7.89 (2H, d, $J=8.8$ Hz), 7.85 (2H, d, $J=8.8$ Hz), 6.94 (2H, d, $J=8.4$ Hz), 6.88–6.83 (4H, m). ^{13}C-NMR (methanol-d_4, 100 MHz) δ: 191.9, 191.4, 163.2, 163.1, 160.4, 152.4, 151.5, 148.5, 139.3, 133.2, 133.1, 129.0, 127.4, 127.3, 126.1, 115.8, 115.0. *Anal.* Calcd for $C_{21}H_{16}N_2O_5\cdot0.8H_2O$: C, 69.90; H, 3.91; N, 6.79. Found: C, 67.50; H, 4.29; N, 6.37.

Synthesis of 5-(Naphthalen-2-yl)-2,3-bis(1-oxo-4-hydroxyphenylmethyl)pyrazine (1b) The deprotection reaction for **7b** was performed using the same procedure as that for obtaining **1a**.[12] After recrystallization from isopropanol/hexane mixed solvent system, **1b** was obtained as yellow solid (56.7 mg, 66%). ^{1}H-NMR (DMSO-d_6, 400 MHz) δ: 9.65 (1H, s), 8.85 (1H, s), 8.31 (1H, d, $J=8.8$ Hz), 8.13–8.09 (2H, m), 8.01 (2H, d, $J=7.6$ Hz), 7.86 (4H, dd, $J=8.8$ Hz and 2.4 Hz),

7.66–7.60 (2H, m). ^{13}C-NMR (DMSO-d_6, 100 MHz) δ: 191.6, 191.3, 163.4, 163.3, 152.5, 151.2, 150.0, 140.5, 134.6, 133.5, 133.2, 133.1, 132.4, 128.8, 127.5, 127.5, 127.4, 127.3, 127.3, 126.6, 123.7, 115.1, 115.0. *Anal.* Calcd for $C_{28}H_{18}N_2O_4 \cdot 0.4H_2O$: C, 75.33; H, 4.06; N, 6.27. Found: C, 74.13; H, 4.20; N, 6.06.

Synthesis of 2,3-Bis(1-oxo-4-hydroxyphenylmethyl)-5-(quinolin-3-yl)pyrazine (1c) The deprotection reaction for **7c** was performed using the same procedure as that for obtaining **1a**.[12] After recrystallization from isopropanol/hexane mixed solvent system, **1c** was obtained as yellow solid (15.2 mg, 16%). ^{1}H-NMR (DMSO-d_6, 400 MHz) δ: 9.65 (1H, d, J = 2.0 Hz), 9.57 (1H, s), 9.21 (1H, d, J = 1.2 Hz), 8.13 (2H, t, J = 7.4 Hz), 7.93–7.87 (5H, m), 7.72 (1H, t, J = 7.4 Hz), 6.88 (2H, t, J = 8.0 Hz). ^{13}C-NMR (DMSO-d_6, 100 MHz) δ: 191.3, 191.1, 163.3, 152.9, 151.1, 148.8, 148.3, 148.1, 140.3, 136.0, 133.5, 133.4, 131.6, 131.1, 129.0, 128.7, 128.2, 128.0, 127.9, 127.8, 127.1, 115,4. *Anal.* Calcd for $C_{27}H_{17}N_3O_4 \cdot 0.9H_2O$: C, 72.48; H, 3.83; N, 9.39. Found: C, 70.00; H, 3.94; N, 8.96.

Synthesis of 3-(4-Hydroxyphenyl)-5,6-bis(1-oxo-4-hydroxyphenylmethyl)pyrazin-2(1*H*)-one (2a) The deprotection reaction for **8a** was performed using the same procedure as that for obtaining **1a**.[12] After recrystallization from isopropanol/hexane mixed solvent system, **2a** was obtained as yellow solid (35.9 mg, 20%). ^{1}H-NMR (methanol-d_4, 400 MHz) δ: 10.57 (1H, s), 10.42 (1H, s), 9.98 (1H, s), 8.24 (2H, d, J = 8.8 Hz), 7.90 (2H, d, J = 8.8 Hz), 7.77 (2H, d, J = 8.4 Hz), 6.87–6.82 (6H, m). ^{13}C-NMR (methanol-d_4, 100 MHz) δ: 188.8, 187.3, 163.4, 162.4, 160.0, 155.7, 133.6, 132.6, 131.1, 128.2, 127.6, 127.0, 116.0, 115.5, 115.4. *Anal.* Calcd for $C_{24}H_{16}N_2O_6 \cdot H_2O$: C, 67.29; H, 3.76; N, 6.54. Found: C, 64.57; H, 3.97; N, 6.18.

Synthesis of 3-(Naphthalen-2-yl)-5,6-bis(1-oxo-4-hydroxyphenylmethyl)pyrazin-2(1*H*)-one (2b) The deprotection reaction for **8b** was performed using the same procedure as that for obtaining **1a**.[12] After recrystallization from isopropanol/hexane mixed solvent system, **2b** was obtained as yellow solid (32.3 mg, 34%). ^{1}H-NMR (DMSO-d_6, 400 MHz) δ: 9.08 (1H, s), 8.20 (1H, d, J = 8.8 Hz), 7.99 (2H, d, J = 8.8 Hz), 7.99 (1H, d, J = 8.0 Hz), 7.76–7.70 (4H, m), 7.38 (2H, quint, J = 6.8 Hz), 6.82 (2H, d, J = 8.8 Hz), 6.79 (2H, d, J = 8.4 Hz). ^{13}C-NMR (DMSO-d_6, 100 MHz) δ: 188.7, 187.1, 164.5, 163.6, 155.3, 141.1, 134.2, 133.2, 132.84, 132.2, 131.6, 130.2, 129.3, 128.9, 128.0, 127.8, 127.5, 126.2, 125.1, 114.2, 113.35, 77.4, 55.4, 55.3. *Anal.* Calcd for $C_{28}H_{18}N_2O_5 \cdot 0.6H_2O$: C, 72.72; H, 3.92; N, 6.06. Found: C, 71.08; H, 4.14; N, 5.88.

Synthesis of 5,6-Bis(1-oxo-4-hydroxyphenylmethyl)-3-(quinolin-3-yl)pyrazin-2(1*H*)-one (2c) The deprotection reaction for **8c** was performed using the same procedure as that for obtaining **1a**.[12] After recrystallization from isopropanol/hexane mixed solvent system, **2c** was obtained as yellow solid (11.2 mg, 13%). ^{1}H-NMR (DMSO-d_6, 400 MHz) δ: 10.59 (1H, s), 10.43 (1H, s), 9.58 (1H, s), 9.40 (2H, s), 8.13 (1H, d, J = 8.0 Hz), 8.07 (1H, d, J = 8.4 Hz), 7.96 (2H, d, J = 8.4 Hz), 7.86–7.77 (3H, m), 7.68 (1H, t, J = 7.4 Hz), 6.89 (2H, d, J = 8.8 Hz), 6.85 (2H, d, J = 8.8 Hz). ^{13}C-NMR (DMSO-d_6, 100 MHz) δ: 188.6, 163.6, 162.6, 150.5, 148.0, 136.7, 133.7, 132.7, 132.1, 131.3, 129.8, 129.2, 128.7, 128.0, 127.8, 127.3, 116.2, 115.7, 115.5. *Anal.* Calcd for $C_{27}H_{17}N_3O_5 \cdot 1.3H_2O$: C, 69.97; H, 3.70; N, 9.07. Found: C, 66.51; H, 3.80; N, 8.31.

Synthesis of (5-(4-Methoxyphenyl)pyrazin-2-yl)(morpholino)methanone (12) A solution of 5-(4-methoxyphenyl)-pyrazine-2-carboxylic acid (**11**,[18] 202 mg, 869 μmol) in $SOCl_2$ (5.0 mL) was refluxed for 3 h. The excess $SOCl_2$ was removed under reduced pressure, and the resulting crude product was once dried *in vacuo*, and then dissolved in 3.0 mL of dichloromethane. To this dichloromethane solution, morpholine (0.30 mL, 3.44 mmol) in 1.3 mL of dichloromethane was added at 0°C. The mixture was stirred at 0°C to room temperature at 15 h, Aqueous Na_2CO_3 solution (2%, 2.5 mL) was added to the reaction mixture, and the organic layer was separated, washed with 3 mL of water, and dried over Na_2SO_4. Removal of the solvent gave the product as orange solids (241 mg, 81%). This material was used directly in the next step without further purification. ^{1}H-NMR ($CDCl_3$, 400 MHz) δ: 8.99 (1H, s), 8.91 (1H, s), 8.03 (2H, d, J = 8.8 Hz), 7.05 (2H, d, J = 8.8 Hz), 3.89 (3H, s), 3.84 (4H, s), 3.76-3.75 (8H, m). ^{13}C-NMR ($CDCl_3$, 100 MHz) δ: 165.6, 161.8, 153.0, 145.7, 145.4, 138.8, 128.8, 128.2, 114.8, 67.2, 67.0, 55.6, 47.9, 43.1. ESI-MS *m/z*: 322.1173 (Calcd for $C_{16}H_{17}N_3NaO_3$ $[M + Na]^+$: 322.1168).

Synthesis of (4-Methoxyphenyl)(5-(4-methoxyphenyl)-pyarzin-2-yl)methanone (13) Under argon atmosphere, magnesium (1.05 mg, 43.2 mmol) was placed in a 30-mL 2-necked flask equipped with a dropping funnel. THF (5.0 mL) was added to the flask, and the suspension was cooled to –15°C. Then, *p*-bromoanisol (1.0 mL, 7.99 mmol) in THF (7.0 mL) was added from the dropping funnel over 20 min, and then the mixture was stirred for 1 h at 70°C. After cooling to room temperature, the resulting Grignard reagent was added to a solution of **12** (102 mg, 0.34 mmol) in THF (8.0 mL) at −100°C. The mixture was then allowed to warm up to room temperature with stirring in a period of 36 h. After completion of the reaction, the reaction mixture was neutralized with 6 M HCl (0.3 mL), and separated between water and chloroform. The organic layer was dried over Na_2SO_4. Removed of the solvent gave **13** as yellow solid (61.5 mg, 56%). ^{1}H-NMR ($CDCl_3$, 400 MHz) δ: 9.23 (1H, s), 9.04 (1H, s), 8.18 (2H, d, J = 8.8 Hz), 8.10 (2H, d, J = 8.8 Hz), 7.07 (2H, d, J = 8.8 Hz), 7.01 (2H, d, J = 8.8 Hz), 3.91 (6H, s). ^{13}C-NMR ($CDCl_3$, 100 MHz) δ: 190.6, 164.0, 162.1, 153.8, 147.6, 145.7, 139.2, 133.5, 129.1, 129.0, 128.3, 114.8, 113.8, 55.6. ESI-MS *m/z*: 343.1052 (Calcd for $C_{19}H_{16}N_2NaO_3$ $[M + Na]^+$: 343.1059). *Anal.* Calcd for $C_{19}H_{16}N_2O_3$: C, 71.24; H, 5.03; N, 8.74. Found: C, 70.86; H, 5.06; N, 8.64.

Synthesis of (4-Hydroxyphenyl)(5-(4-hydroxypheny)pyrazin-2-yl)methanone (10) Pyridine hydrochloride (4.37 g, 37.8 mmol) was heated to 210°C, **13** (61.3 mg, 0.191 mmol) was added, and the mixture was kept at this temperature for 2 h. Then, the reaction mixture was poured on to ice, and organic materials were extracted with AcOEt. The combined organic extracts were dried over Na_2SO_4, and evaporated. The product was obtained as orange solid (69.7 mg, quant.). For data collection, this material was recrystallized from methanol. ^{1}H-NMR (DMSO-d_6, 400 MHz) δ: 10.55 (1H, s), 10.13 (1H, s), 9.25 (1H, d, J = 1.0 Hz), 9.05 (1H, d, J = 1.0 Hz), 8.13 (2H, d, J = 8.6 Hz), 7.99 (2H, d, J = 8.6 Hz), 6.95 (2H, d, J = 8.6 Hz), 6.90 (2H, d, J = 8.6 Hz). ^{13}C-NMR (DMSO-d_6, 100 MHz) δ: 189.8, 162.6, 160.2, 152.8, 147.3, 144.6, 139.0, 133.4, 129.0, 127.0, 125.9, 116.1, 115.1. *Anal.* Calcd for $C_{17}H_{12}N_2O_3 \cdot 0.7CH_3OH$: C, 67.55; H, 4.74; N, 8.90. Found: C, 67.76; H, 4.60; N, 8.66.

X-Ray Structure Determination A single crystal of **1b** was mounted on the top of a glass fiber, and the data collection was carried out on a Bruker SMART diffractometer

Table 5. The Crystallographic Data of **1b**

Empirical formula	$C_{29}H_{22}N_2O_5$
Formula weight	478.49
Crystal system	Triclinic
Space group	*P*-1
Unit cell dimensions	$a = 7.3554(6)$ Å, $b = 11.6050(10)$ Å, $c = 14.4957(13)$ Å
	$\alpha = 73.0552(15)°$, $\beta = 77.1608(16)°$, $\gamma = 84.8397(17)°$
Volume	1153.61(17) Å^3
Z	4
Density (calculated)	1.377 Mg/m^3
Absorption coefficient	0.095 mm^{-1}
F(000)	500
Theta range for data collection	1.84 to 27.48°
Index ranges	$-8 <= h <= 9$, $-13 <= k <= 15$, $-18 <= l <= 18$
Reflections collected	7350
Independent reflections	5245 [R(int) = 0.0262]
Completeness to theta = 27.48°	98.9%
Absorption correction	Empirical
Max. and min. transmission	0.9964 and 0.9834
Refinement method	Full-matrix least-squares on F^2
Data/restraints/parameters	5245/0/329
Goodness-of-fit on F^2	1.045
Final R indices [$I > 2\sigma(I)$]	$R_1 = 0.0890$, $wR_2 = 0.2242$
R indices (all data)	$R_1 = 0.1380$, $wR_2 = 0.2584$
Largest diff. peak and hole	1.220 and -0.495 e·Å^{-3}

$R_1 = \Sigma(|F_0|-|F_c|)/\Sigma|F_0|$; $wR_2 = [\Sigma w(|F_0|-|F_c|)^2/\Sigma_w F_0^2]^{1/2}$.

equipped with a CCD area detector at 100 K. The data were corrected for Lorentz and polarization effects, and absorption corrections were applied with the *SADABS* program.[39] The structure was solved by direct methods and subsequent difference Fourier syntheses using the program *SHELXTL*.[40] All non-H atoms were refined anisotropically, and H atoms were placed in calculated positions and thereafter refined with $U_{iso}(H) = 1.2U_{eq}(C)$. The obtained cystallographic data are summarized in Table 5.

***In Vitro* AR Inhibitory Assay**[11] Enzyme activity was measured by monitoring the decay in absorbance at 340 nm, which accompanies the oxidation of NADPH catalyzed by recombinant human AR. The reaction mixture contained 0.2 M phosphate buffer (pH 6.2), 1.5 mM NADPH, 100 mM D,L-glyceraldehyde, and 3.6 μU/mL AR, in a total volume of 1.0 mL. All the above reagents, except D,L-glyceraldehyde, were incubated at 25°C for 3 min. The reaction was initiated by the addition of D,L-glyceraldehyde, and it was monitored spectrophotometrically for 3 min at the same temperature. Inhibitory activity was tested in the above assay conditions by including the in the inhibitors dissolved in dimethyl sulfoxide (DMSO) at desired concentrations in the reaction mixture. The final concentration of DMSO in the reaction mixture was kept at a constant concentration of 0.3%. Reference blank assay, lacking either the substrate or enzyme, were routinely included; the rates were subtracted from the reaction rates, to correct for the nonenzymatic oxidation of NADPH. IC_{50} values, which express the inhibitor concentrations that produce the 50% inhibition on the oxidation of NADPH catalyzed by the AR, were calculated using a log linear regression analysis of the log dose-inhibition plots. Each plot was provided using at least three concentrations of inhibitor with two replicates at each concentration.

Docking Study All docking simulations were performed using the GOLD Suite software package (ver. 5.6.1). ChemPLP scoring function was used to predict the docking poses, and the obtained poses were rescored with Astex Statistical Potential (ASP),[36] known as a good scoring function for proteins making specific hydrogen bonds with ligands.[37] The best pose for each ligand was determined by considering the results obtained with both of these scoring functions (both ChemPLP and ASP scores give positive values, with the higher score indicating the more likely pose). The protein structures were obtained from the Protein Data Bank (PDB). The optimized structures and atom charges of the selected ligands for the docking simulations were calculated by the semi-empirical PM7 calculation method.[30] All docking poses were visualized by the Hermes software package (ver. 1.9.1) from the Cambridge Crystallographic Data Centre (CCDC).

Acknowledgments This research was supported by JSPS KAKENHI Grant Number JP25410179. Partial financial support to RS by the Faculty of Science Special Grant for Promoting Scientific Research at Toho University is also gratefully appreciated.

Conflict of Interest The authors declare no conflict of interest.

Supplementary Materials The online version of this article contains supplementary materials.

References

1) American Diabetes Association, *Diabetes Care*, **32** (Supplement_1), S62–S67 (2009).
2) Maccari R., Ottana R., *J. Med. Chem.*, **58**, 2047–2067 (2015).
3) Brownlee M., *Nature* (London), **414**, 813–820 (2001).
4) Changjin Z., Aldose reductase inhibitors as potential therapeutic

drugs of diabetic complications, "Diabetes Mellitus—Insights and Perspectives," ed. by Oguntibeju O., InTech, London, 2013, pp. 17–46.
5) Kador P. F., Kinoshita J. H., Sharpless N. E., *J. Med. Chem.*, **28**, 841–849 (1985).
6) Pfeifer M. A., Schumer M. P., *Diabetes*, **44**, 1355–1361 (1995).
7) Costantino L., Rastelli G., Cignarella G., Vianello G., Barlocco D., *Expert Opin. Ther. Pat.*, **7**, 843–858 (1997).
8) Costantino L., Rastelli G., Gamberini M. C., Barlocco D., *Expert Opin. Ther. Pat.*, **10**, 1245–1262 (2000).
9) Miyamoto S., *Chem-Bio Informatics J.*, **2**, 74–85 (2002).
10) Durán R., Zubía E., Ortega M., Naranjo S., Salvá J., *Tetrahedron*, **55**, 13225–13232 (1999).
11) Saito R., Tokita M., Uda K., Ishikawa C., Satoh M., *Tetrahedron*, **65**, 3019–3026 (2009).
12) Buron F., Ple N., Turck A., Queguiner G., *J. Org. Chem.*, **70**, 2616–2621 (2005).
13) Darren M., Gordon K. P., James M. W., U.S. Patent 11913114 (2006).
14) Duffy K. J., Chai D., Colon M., Fitch D. M., King S. R., Shaw A. N., Tedesco R., Wiggall K., Johnson N. W., Kasparec J., Zimmerman M. N., Int. Patent WO 132739 (2006).
15) Cramer N., Laschat S., Baro A., Schwalbe H., Richter C., *Angew. Chem. Int. Ed.*, **44**, 820–822 (2005).
16) Scott W. J., Stille J. K., *J. Am. Chem. Soc.*, **108**, 3033–3040 (1986).
17) Kotsuki H., Datta K. P., Hayakawa H., Suenaga H., *Synthesis*, **1995**, 1348–1350 (1995).
18) Mahboobi S., Sellmer A., Burgemeister T., Lyssenko A., Schollmeyer D., *Monatsh. Chem.*, **135**, 333–342 (2004).
19) La Motta C., Sartini S., Salerno S., Simorini F., Taliani S., Marini A. M., Da Settimo F., Marinelli L., Limongelli V., Novellino E., *J. Med. Chem.*, **51**, 3182–3193 (2008).
20) Manzanaro S., Salvá J., de la Fuente J. Á., *J. Nat. Prod.*, **69**, 1485–1487 (2006).
21) Kato K., Nakayama K., Mizota M., Miwa I., Okuda J., *Chem. Pharm. Bull.*, **39**, 1540–1545 (1991).
22) Rastelli G., Vianello P., Barlocco D., Costantino L., DelCorso A., Mura U., *Bioorg. Med. Chem. Lett.*, **7**, 1897–1902 (1997).
23) Oka M., Matsumoto Y., Sugiyama S., Tsuruta N., Matsushima M., *J. Med. Chem.*, **43**, 2479–2483 (2000).
24) Maccari R., Ottana R., Ciurleo R., Rakowitz D., Matuszczak B., Laggner C., Langer T., *Bioorg. Med. Chem.*, **16**, 5840–5852 (2008).
25) Sotriffer C. A., Kramer O., Klebe G., *Proteins*, **56**, 52–66 (2004).
26) Steuber H., Zentgraf M., La Motta C., Sartini S., Heine A., Klebe G., *J. Mol. Biol.*, **369**, 186–197 (2007).
27) Maccari R., Ottanà R., Ciurleo R., Vigorita M., Rakowitz D., Steindl T., Langer T., *Bioorg. Med. Chem. Lett.*, **17**, 3886–3893 (2007).
28) Chen X., Zhu C., Guo F., Qiu X., Yang Y., Zhang S., He M., Parveen S., Jing C., Li Y., Ma B., *J. Med. Chem.*, **53**, 8330–8344 (2010).
29) Cousido-Siah A., Ruiz F. X., Mitschler A., Porte S., de Lera A. R., Martin M. J., Manzanaro S., de la Fuente J. A., Terwesten F., Betz M., Klebe G., Farres J., Pares X., Podjarny A., *Acta Crystallogr. D Biol. Crystallogr.*, **70**, 889–903 (2014).
30) Stewart J. J. P., *J. Mol. Model.*, **19**, 1–32 (2013).
31) Klamt A., Schuurmann G., *J. Chem. Soc., Perkin Trans.*, **2**, 799–805 (1993).
32) Saito R., Hirano T., Maki S., Niwa H., *J. Photochem. Photobiol. Chem.*, **293**, 12–25 (2014).
33) Gold Version 5.2; The Cambridge Crystallographic Data Centre (CCDC): Cambridge, U.K. ‹http://www.ccdc.cam.ac.uk›.
34) Verdonk M. L., Cole J. C., Hartshorn M. J., Murray C. W., Taylor R. D., *Proteins*, **52**, 609–623 (2003).
35) Korb O., Stützle T., Exner T. E., *J. Chem. Inf. Model.*, **49**, 84–96 (2009).
36) Mooij W. T. M., Verdonk M. L., *Proteins*, **61**, 272–287 (2005).
37) Cambridge Crystallographic Data Centre, 'Gold Scoring Function Performance against the Dud Decoy/active Set, 2012.': ‹https://www.ccdc.cam.ac.uk/support-and-resources/ccdcresources/VS_workcase.pdf› (14.09.16).
38) Saito R., Hoshi M., Kato A., Ishikawa C., Komatsu T., *Eur. J. Med. Chem.*, **125**, 965–974 (2017).
39) Sheldrick G. M., Program for absorption correction of area detector frames, Bruker AXS, Inc., Madison, WI, 1996.
40) SHELXTL, version 5.1, Bruker AXS Inc., Madison, WI, 1997.